

## CO oxidation on electrically charged gold nanotips

J.-S. McEwen and P. Gaspard

*Center for Nonlinear Phenomena and Complex Systems,  
Université Libre de Bruxelles, Code Postal 231, Campus Plaine, B-1050 Brussels, Belgium*

We report a study of the oxidation of CO on a gold nanotip in the presence of high electrostatic fields. With the binding energies obtained using density functional theory (DFT) as a function of the electric field, a simple field-dependent kinetic model based on the Langmuir-Hinshelwood mechanism is set up. We show that the dissociative adsorption of oxygen on gold happens only below a negative critical value of the electric field while the binding of CO on gold is enhanced for positive values. We explain the propagation of a wave observed in FIM experiments and predict that the oxidation of CO occurs on negatively charged gold clusters.

PACS numbers: 31.15.Ew, 68.35.Md, 68.43.Bc, 68.43.-h, 82.65.+r

### I. INTRODUCTION

Gold is the noblest among metals and was regarded chemically inert for centuries. Notwithstanding the low chemical reactivity, oxygen adsorption on gold has gained considerable interest in the context with the research by Haruta *et al.* [1, 2] which demonstrated a high activity in the CO oxidation over Au nanoparticles of 1-6 nanometers supported on metal oxides at relatively low temperatures. While the mechanism of this catalytic reaction is not yet fully understood, some important experimental and theoretical efforts have been undertaken [3, 4]. In particular, recent DFT calculations have shown that when Au clusters adsorb at oxygen-vacancy sites on a Mg(001) surface a charge transfer occurs from the oxide to the metal cluster and makes the clusters more catalytically active [5, 6]. The O<sub>2</sub> molecules in the gas phase have then been shown to adsorb on these catalytically active sites as a peroxy-type species (O-O bond parallel to the surface) with a binding energy up to 1.85 eV [5, 6]. Other charge transfer mechanisms have been reported when Au is supported on a TiO<sub>2</sub> surface [7].

Several reaction mechanisms have been proposed in the formation of CO<sub>2</sub> on these gold supported clusters [4, 5]. One has the CO molecule brought to the vicinity of an adsorbed O<sub>2</sub> molecule so as to react spontaneously and form a CO<sub>2</sub> molecule [5]. Another has the oxygen molecule adsorb dissociatively and then oxidize an adsorbed CO adparticle [4]. Finally, another possibility has the O<sub>2</sub> molecule adsorbing on the Au cluster to react with an adsorbed CO molecule to form a CO<sub>2</sub> and an O product [4, 5]. The latter reaction pathway has been determined to be more facile when the gold cluster is supported by a TiO<sub>2</sub> oxide surface [4, 7]. In any case, the presence of a metal oxide substrate has been determined to be essential to the dissociative adsorption of O<sub>2</sub> on Au clusters: The absence of the oxide would present a large dissociative activation barrier for the O<sub>2</sub> molecule and greatly hinder its molecular adsorption on gold [8].

Recently, the interaction of carbon monoxide and oxygen with gold has also been investigated with field emission techniques [9–11]. These studies have shown that, on a positively charged gold nanotip, carbon monoxide adsorbs on gold to form mono- and di-carbonyls although oxygen neither adsorbs nor dissociates [9–11]. In these experiments, a potential difference is applied between a thin gold needle and a screen. The radius of curvature at the tip of the needle may be as small as about  $R \simeq 20\text{-}30$  nm so that huge electric fields of the order of ten Volts per nanometer can be reached [12–14]. Such high electric fields deeply modify the electronic orbitals and may induce new reaction pathways. The electric field can be either positive in Field Ion Microscopy (FIM) or negative in Field Emission Microscopy (FEM), as schematically depicted in Fig. 1. Accordingly, a reaction channel which is closed at certain values of the electric field may open at other positive or negative values. This remark has motivated our systematic study of the interaction of oxygen with gold in both negative and positive electric fields by DFT calculations.

The purpose of the present paper is to present a kinetic model of CO oxidation on gold nanotips in positive and negative electric fields and at low and high CO and O<sub>2</sub> pressures. The interaction of CO with gold is modeled as in our previous study of the formation of a wave during the adsorption of CO on gold under FIM conditions [11]. In the present paper, the dissociative adsorption of oxygen on gold is modeled as well and considered to occur directly from the gas phase, i.e., we will not consider the possibility of adsorbed O<sub>2</sub> molecules. We will use DFT calculations to determine the dependence of the adsorption and desorption rate constants on the electric field. These constants will then be incorporated in a complete kinetic model of CO oxidation under FIM and FEM conditions based on the Langmuir-Hinshelwood mechanism. Since the electric field locally varies on the surface of a metallic tip according to

its radius of curvature, the adsorption and desorption of carbon monoxide and oxygen will be spatially modulated along the surface and can change by orders of magnitude with the electric field. Moreover, the present kinetic model will capture experimental observations under quite different conditions. Specifically, at positive electric fields and low pressures (from  $1 \times 10^{-7}$  to  $1 \times 10^{-2}$  mbar) we will show that the model reproduces the experimentally observed wave propagation of CO [11] along with the absence of oxygen dissociation and CO oxidation [10]. In contrast, the model will illustrate that CO oxidation becomes possible at negative electric fields if the pressure of CO and O<sub>2</sub> is as high as in the experiments where CO oxidation was observed [2].

The plan of the paper is the following. The kinetic model is presented in Sec. II. The determination of the rate constants from DFT calculations and experimental measurements is carried out in Sec. III for oxygen and in Sec. IV for CO. We show that this model explains the formation of the observed wave in Sec. V and the oxidation of CO in Sec. VI. Conclusions are drawn in Sec. VII.

## II. KINETIC MODEL

### A. Electric field on the surface

The relatively large diffusivity of gold atoms on its own surface tends to blur the crystalline structures at room temperature, which are not prominent in images of gold tips, contrary to the cases of other metals such as platinum or tungsten. In this regard, the tip of the gold needle can be supposed to form a relatively smooth surface of the shape of a paraboloid.

Since the needle is metallic, the electric field  $F$  is perpendicular to the surface. The field is highest at the apex, i.e., on the axis of the paraboloid, and decreases away from the axis in the flanks of the needle. As shown in the literature [14], the electric field is proportional to the surface density of electric charges. The dependence on the position is given by [14]

$$F = \frac{F_0}{\sqrt{1 + \frac{r^2}{R^2}}} \quad (1)$$

where  $r$  is the radial distance between a point on the surface of the paraboloid and its axis,  $F_0$  is the value of the electric field at the apex, and  $R$  is the radius of curvature of the tip at the apex. Figure 1 illustrates the type of systems we envisage. We notice that we here have a model for an electrically charged gold nanocluster supported on an oxide as shown in Fig. 1(c) for which the field is at its strongest at the metal/metal oxide interface.

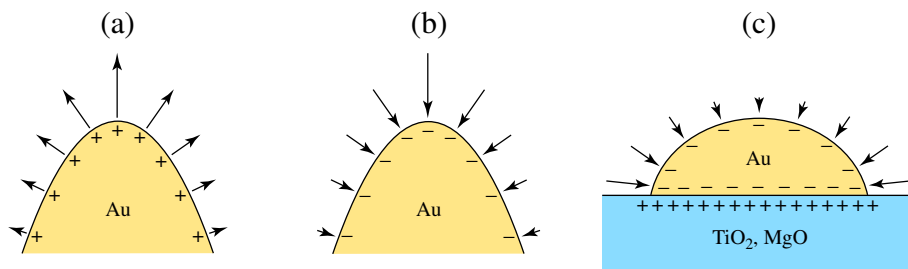


FIG. 1: Schematic representation of three systems described in the text: (a) Positively charged gold tip in FIM; (b) Negatively charged gold tip in FEM; (c) Negatively charged gold cluster on an oxide solid substrate. We notice that the electric field is proportional to the surface density of electric charges on the conductor.

### B. Enhancement of the pressures due to the electric field

The gold nanotip is submitted to a mixture of O<sub>2</sub> or CO gases. Because of the polarizability of O<sub>2</sub> and CO molecules and the electric dipole of CO (see Table I), their pressures are enhanced in the presence of the electric field around the tip with respect to the pressures measured at the gauge where the electric field can be supposed to vanish [15]. The equilibrium statistical mechanics of diatomic molecules in an electric field can be used to obtain the dependence of the pressure on the electric field  $F$ . Using a similar approach to Ref. [15], the effective potential of the molecules

molecule	$d$ (Debye)	$\alpha_{\parallel}$ ( $4\pi\epsilon_0\text{\AA}^3$ )	$\alpha_{\perp}$ ( $4\pi\epsilon_0\text{\AA}^3$ )
O <sub>2</sub>	0	2.33	1.23
CO	0.11	2.33	1.80

TABLE I: Experimental values of the electric dipole and polarizabilities for the O<sub>2</sub> and CO molecules [17]. The electric dipole of CO is oriented toward the oxygen atom which unexpectedly carries a small positive charge. The unit of electric dipole is 1 Debye =  $3.33564 \cdot 10^{-30}$  C m and  $\epsilon_0$  is the vacuum permittivity.

is obtained as a function of the applied field [16]. Figure 2(a) depicts this effective potential. At  $T = 300$  K, these effective potentials can be approximated by a quadratic function of the field according to

$$P_{\text{O}_2}(F) \simeq P_{\text{O}_2}(0) e^{\beta \tilde{\alpha}_{\text{eff}} F^2 / 2} \quad \text{with} \quad \frac{1}{2} \beta \tilde{\alpha}_{\text{eff}} F^2 = -\beta \tilde{u}_{\text{eff}} \simeq 0.022 \text{ (V/nm)}^{-2} F^2 \quad (2)$$

$$P_{\text{CO}}(F) \simeq P_{\text{CO}}(0) e^{\beta \alpha_{\text{eff}} F^2 / 2} \quad \text{with} \quad \frac{1}{2} \beta \alpha_{\text{eff}} F^2 = -\beta u_{\text{eff}} \simeq 0.028 \text{ (V/nm)}^{-2} F^2 \quad (3)$$

where  $\beta = (k_{\text{B}}T)^{-1} = 38.68169 \text{ eV}^{-1}$ . The enhancement factor of the pressure due to the electric field is depicted in Fig. 2(b), which shows that the pressure is multiplied by about 9.5 for O<sub>2</sub> and 17 for CO in an electric field of 10 V/nm.

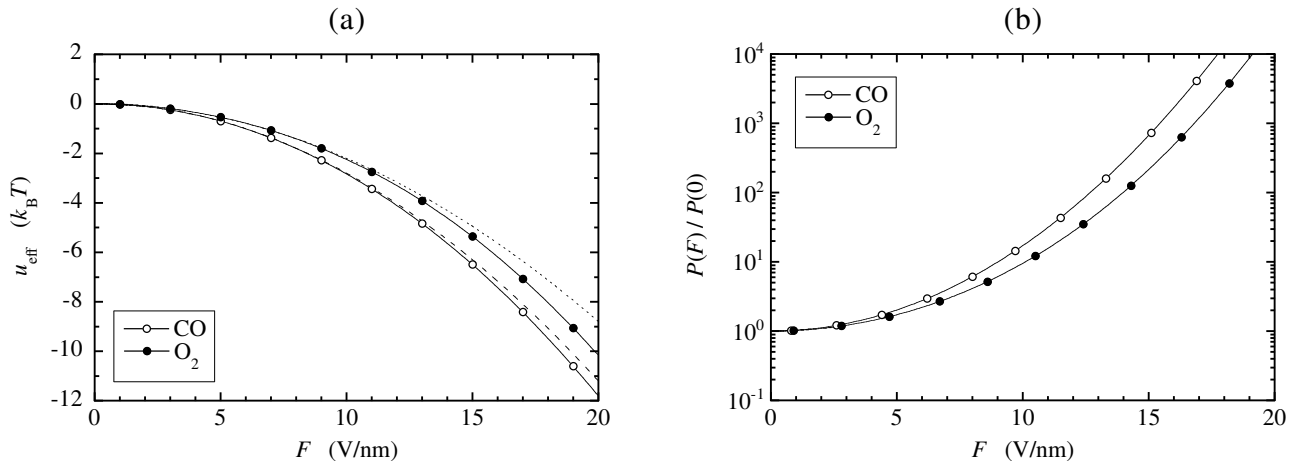
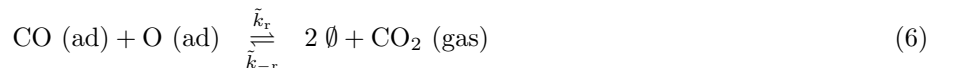


FIG. 2: (a) Effective potential due to the electric polarizability and dipole versus the electric field  $F$  for O<sub>2</sub> (filled circles) and CO (open circles) at  $T = 300$  K, and compared with the approximations (2) and (3) (dashed lines). (b) The ratio  $P(F)/P(0)$  of the pressure in an electric field to the pressure without electric field for O<sub>2</sub> (filled circles) and CO (open circles) versus the electric field  $F$  at  $T = 300$  K.

### C. Reaction network and the kinetic model

We consider the Langmuir-Hinshelwood mechanism of oxidation:



where  $\emptyset$  denotes an empty adsorption site on the surface.  $\tilde{k}_{\text{a}}$  and  $k_{\text{a}}$  are the constants of adsorption of O<sub>2</sub> and CO respectively.  $\tilde{k}_{\text{d}}$  and  $k_{\text{d}}$  are the corresponding constants of desorption.  $k_{\text{r}}$  and  $k_{-\text{r}}$  are the reaction constants of CO

process	constant	$k_x^0$	$E_x^\ddagger$ (eV)
O <sub>2</sub> dissociative adsorption	$\tilde{k}_a$	500 Pa <sup>-1</sup> s <sup>-1</sup>	$2.15 + 0.53 F + 0.0175 F^2 - 0.0023 F^3$
O <sub>2</sub> associative desorption	$\tilde{k}_d$	$9 \cdot 10^{12}$ s <sup>-1</sup>	$1.45 + 0.28 F + 0.0125 F^2 - 0.0018 F^3$
CO adsorption	$k_a$	700 Pa <sup>-1</sup> s <sup>-1</sup>	0
CO desorption	$k_d$	$2.78 \cdot 10^{14}$ s <sup>-1</sup>	$0.55 + 0.055 F + 0.0048 F^2$
CO oxidation	$k_r$	$10^{12}$ s <sup>-1</sup>	0.59

TABLE II: Values of the prefactors  $k_x^0$  and activation energies  $E_x^\ddagger$  entering into the reaction constants  $k_x = k_x^0 \exp(-E_x^\ddagger/k_B T)$  of the kinetic model (7)-(8). The electric field  $F$  is in V/nm. Notice that the value of  $k_{-r}$  does not need to be specified since it is here assumed that  $P_{CO_2} = 0$ .

oxidation. These constants depend on the temperature which is supposed to be homogeneous and equal to  $T = 300$  K. The essential aspect of the system is that the rate constants depend on the electric field, which varies along the surface. Therefore, the system is not homogeneous because of the spatial dependence of the electric field as given in Eq. (1).

To model the above processes one must set up a kinetic lattice gas model. This is done by specifying the appropriate occupation numbers and transition probabilities that enter into the master equation. The equations of evolution of oxygen and carbon monoxide can then be readily obtained in terms of their respective average occupations at each site. The reaction constants in Eqs. (4), (5), and (6) that enter into the transition probabilities can also be automatically adjusted to satisfy the detailed balance conditions, as was done in Ref. [18] for a single adsorbate species. However, here we shall not be concerned with hopping processes, i.e., we shall assume that the oxygen atoms and the carbon monoxide molecules are immobile on the surface (a reasonable approximation since the main experimental features will be reproduced within our model).

The corresponding mean field equations of evolution in terms of the partial coverages of oxygen ( $\theta_O$ ) and carbon monoxide ( $\theta_{CO}$ ), which will be used in our modeling, are given by

$$\frac{d\theta_O}{dt} = 2\tilde{k}_a P_{O_2} (1 - \theta_{CO} - \theta_O)^2 - 2\tilde{k}_d \theta_O^2 - k_r \theta_{CO} \theta_O + k_{-r} P_{CO_2} (1 - \theta_{CO} - \theta_O)^2 \quad (7)$$

$$\frac{d\theta_{CO}}{dt} = k_a P_{CO} (1 - \theta_{CO} - \theta_O) - k_d \theta_{CO} - k_r \theta_{CO} \theta_O + k_{-r} P_{CO_2} (1 - \theta_{CO} - \theta_O)^2 \quad (8)$$

where  $P_{CO_2}$  is the pressure of the gas phase and here we have neglected all lateral interactions. Since the CO<sub>2</sub> gas is evacuated out of the reactor chamber, its pressure will vanish,  $P_{CO_2} = 0$ . This allows us to simplify our evolution equations by eliminating the last term of Eq. (7) and the corresponding one of Eq. (8). In the rest of the paper, we will assume that the condition  $P_{CO_2} = 0$  holds. The values of the other parameters in Eqs. (7)-(8) are given in Table II and explained below.

The very high electric fields that are attainable with field emission techniques will strongly affect the electronic structure of the adsorbed species and thus the reaction constants appearing in Eqs. (7)-(8). Indeed, the binding energies of the adsorbates as well as the energies of the transition states are modified by such large electric fields which are reaching the value of the electric field inside the atoms and molecules. We consider Arrhenius' dependencies on the activation energies,  $k_x = k_x^0 \exp[-\beta E_x^\ddagger(F)]$ , which allows us to obtain the field dependence of the rate constants from the field dependence of the activation energies which can be inferred from DFT calculations.

We also notice that the system of ordinary differential equations (7)-(8) depends on the position via the electric field: The rate constants as well as the pressures depend on the electric field which itself varies in space according to Eq. (1). The adsorption, desorption, and reaction processes do not advance at the same speed at every location of the surface. As a consequence, the time evolution of the system is highly inhomogeneous along the surface of the needle from its apex to its flanks, albeit with a preserved cylindrical symmetry. Moreover, the electric field (1) drops to a negligible value in the flanks beyond a distance  $r$  of the order to the radius of curvature  $R$ .

#### D. CO oxidation

It can be shown, when using the element of area on the surface of a paraboloid, that total yield of CO oxidation is given by

$$Y_{\text{tot}} = \frac{2\pi}{a_s} \int_0^{r_{\text{max}}} k_r \theta_{CO} \theta_O \sqrt{1 + \frac{r^2}{R^2}} r dr \quad (9)$$

where  $a_s$  is the area of a site on the surface and  $r_{\max}$  is the maximum distance at which the paraboloid is cut. For a long needle, we can take  $r_{\max} = \infty$ . At  $T = 300$  K, gold forms a fcc crystal with an inter-atomic distance of  $d = 2.9$  Å, from which we can estimate that  $a_s \simeq (\sqrt{3}/2)d^2 \simeq 7$  Å<sup>2</sup>.

The total yield will be governed by the reaction in Eq. (6). This is an activated process with the rate constant:

$$k_r = k_r^0 e^{-\beta E_r^\ddagger} \quad (10)$$

The energy barrier of CO oxidation on a gold surface is known to be  $E_r^\ddagger = 57$  kJ/mol = 0.59 eV [19]. The attempt frequency is taken to be  $k_r^0 = 10^{12}$  s<sup>-1</sup>. We do not assume in the present model a special dependence of the activation barrier on the electric field. This does not seem essential to reproduce the current experimental observations.

### E. DFT calculations

In order to determine the activation energies of adsorption and desorption, DFT calculations were carried out with the adsorbates on gold clusters  $Au_n$ . The DFT calculations were performed with the B3LYP method of the Gaussian03 software with their basis sets LanL2DZ for Au and 6-311G\*\* for O and CO.

Gold clusters  $Au_n$  of size  $1 \leq n \leq 9$  have been successively built as in Ref. [11]. Gold clusters  $Au_n$  with odd  $n$  are in a doublet state. Thereafter, an oxygen atom or a CO molecule was added to the gold cluster. Figure 3 depicts typical configurations. CO- $Au_n$  and O- $Au_n$  with odd  $n$  are also found in a doublet ground state.

We notice that, in CO- $Au_n$ , the carbon atom is in direct contact with gold at a distance of about 2 Å. The oxygen atom is at a distance of 1.14 Å from carbon and thus further away from the gold surface. The CO bond is not perpendicular to the surface but tilted.

On the other hand, similar DFT calculations were carried out for the isolated molecular species O<sub>2</sub> and CO. The difference of energies was used to determine their binding energy and this for different values of the electric field which is oriented perpendicular to the cluster surface, as illustrated in Fig. 3. The geometry is optimized in all cases, i.e. in the presence and in the absence of an electric field.

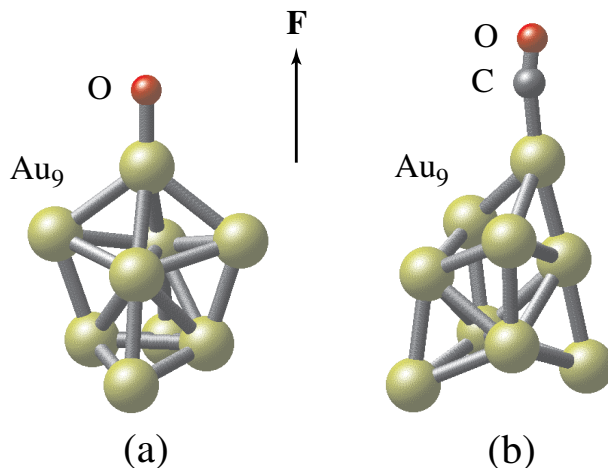


FIG. 3: (a) Configuration of O adsorbed on a gold cluster  $Au_9$ . (b) Configuration of CO adsorbed on a gold cluster  $Au_9$ . The direction of the positive electric field  $\mathbf{F}$  is indicated.

### III. DISSOCIATIVE ADSORPTION AND DESORPTION OF OXYGEN

In this section, we determine the adsorption-desorption rate constants of oxygen on gold. These rates are to be used in Eq. (7) of the kinetic model (4)-(6). For this purpose, we use DFT calculations as well as complementary data from temperature programmed desorption (TPD) experiments.

It is well known that gold does not oxidize at room temperature and in zero electric field, which means that no chemisorption of oxygen occurs under such conditions. This is confirmed by DFT calculations [10, 20, 21] and is summarized in Fig. 4(a). The physisorption of molecular oxygen O<sub>2</sub> on gold is weak with a binding energy of 0.1-0.6

eV which depends on the binding site. At zero electric field,  $F = 0$ , the binding energy of atomic oxygen O on gold is 2.33 eV [10, 20]. Accordingly, two O-Au<sub>n</sub> bonds have an energy of 4.66 eV, which is lower than the electronic dissociation energy 5.3 eV of the two oxygen atoms in the O<sub>2</sub> molecule. Therefore, the dissociative chemisorption of oxygen does not happen as seen in Fig. 4(a). It turns out that the situation is worse in a positive electric field where the binding energy of atomic oxygen on gold is lowered further [10].

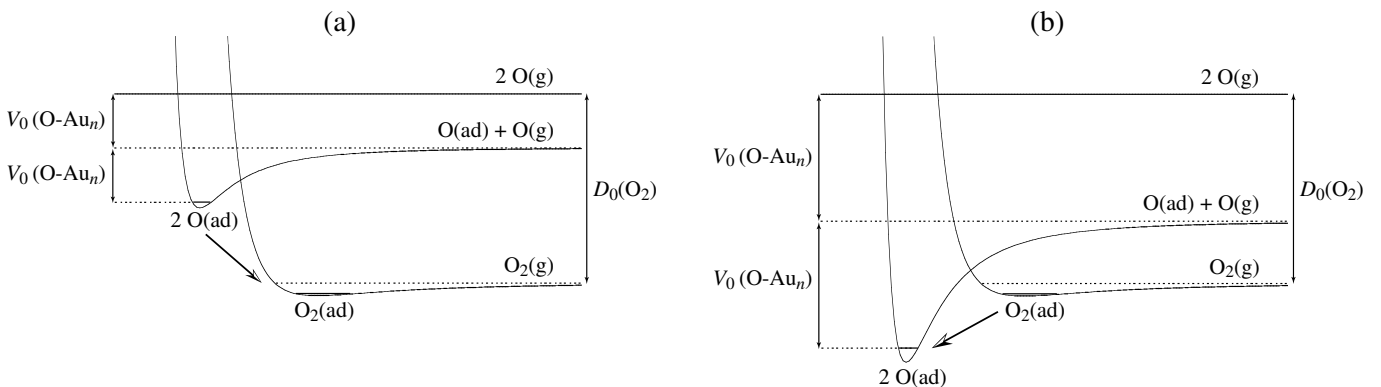


FIG. 4: Schematic diagrams of the potential energy surface of molecular and atomic oxygen above a gold surface: (a) in a zero or positive electric field  $F \geq 0$ ; (b) in a negative electric field below the dissociation threshold  $F < F_c < 0$ .  $D_0(\text{O}_2)$  denotes the energy to dissociate molecular oxygen in the gas phase and  $V_0(\text{O} - \text{Au}_n)$  is the binding energy of atomic oxygen on a the gold surface, both with respect to their zero-point energy. X(g) denotes the species X in the gas phase and X(ad) the species X adsorbed on the surface.

In contrast, one might expect that, when the electric field becomes *negative* the binding energy of oxygen on gold would then increase. If this was the case, the formation of two bonds of atomic oxygen with gold could become energetically favored with respect to molecular oxygen below a certain negative critical field  $F < F_c < 0$ , as shown in Fig. 4(b). In this case, the dissociative chemisorption of oxygen happens, which opens the pathway to the Langmuir-Hinshelwood reactions given in Eqs. (4)-(6) and, in particular, the oxidation of CO if the latter is present on the surface as well.

The negative electric field conjecture is confirmed by our DFT calculations. Figure 5 depicts the binding energy of O-Au<sub>n</sub> → O + Au<sub>n</sub> in the presence of an electric field without any zero point energy corrections:

$$V_e(\text{O-Au}_n; F) = E(\text{O}; F) + E(\text{Au}_n; F) - E(\text{O-Au}_n; F) \quad (11)$$

for  $n = 1$  and  $n = 9$ , which is compared with half the electronic dissociation energy of molecular oxygen

$$\frac{1}{2} D_e(\text{O}_2; F) = E(\text{O}; F) - \frac{1}{2} E(\text{O}_2; F) \quad (12)$$

The latter differs from the standard dissociation energy  $D_0$  (5.12 eV for O<sub>2</sub>) to be found in the tables by the zero point energy; e.g. for a diatomic molecule we have  $D_e = D_0 + \hbar\omega_{\text{vib}}/2$  where  $\omega_{\text{vib}}$  is its vibrational frequency. The electronic dissociation energy is also a quadratic function of the electric field due to the polarizability of molecular oxygen:

$$D_e(\text{O}_2; F) = D_e(\text{O}_2; F = 0) + \frac{1}{2}\alpha_{\parallel} F^2 \quad (13)$$

the electric field being here taken parallel to the internuclei axis. The electric field is also parallel to the O-Au<sub>n</sub> bond which is essentially perpendicular to the gold surface. We observe in Fig. 5 that, indeed, both energies become equal at a critical negative electric field  $F_c$  which depends on the cluster size. It is about  $F_c = -13.4$  V/nm for  $n = 1$  and shifts to  $F_c = -2.7$  V/nm for a larger cluster of  $n = 9$ . As seen in Fig. 5, the dependence of the binding energy of atomic oxygen on gold on the electric field is very strong. This is due to the strong dipolar character of the O-Au<sub>n</sub> bond which can be explained in terms of the electronegativity of oxygen. Accordingly, the electric dipole vector  $\mathbf{d}$  points toward the gold surface. The energy of this dipole is thus  $v_{\text{dip}} = -\mathbf{F} \cdot \mathbf{d}$ . In a positive electric field, the dipole is antiparallel so that the dipolar contribution to energy is positive which weakens the bond thus decreasing the binding energy, as in Fig. 4(a). In a negative electric field, the dipole is parallel and the dipolar contribution to energy is negative which strengthens the bond, favoring chemisorption over physisorption as depicted in Fig. 4(b).

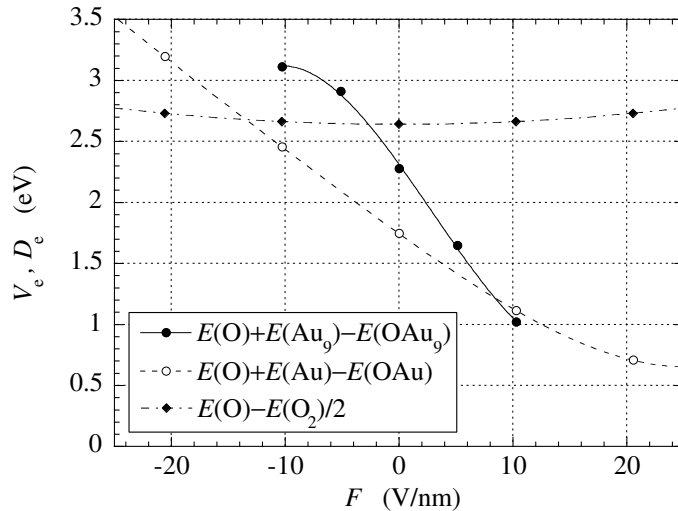


FIG. 5: Binding energy (11) of O on gold  $Au_n$  versus the electric field  $F$  for  $n = 1$  and  $n = 9$ , compared with half the dissociation energy of molecular oxygen (12).

This explains that molecular oxygen undergoes a dissociative chemisorption only below a negative critical electric field. Above this threshold  $F > F_c$ , the molecular oxygen from the gas does not dissociate for the aforementioned energetic reason and either remains as such in the gas or is physisorbed when the temperature is low enough.

In order to model both sub- and super-critical situations, we have to introduce field-dependent energy barriers for adsorption:

$$\tilde{k}_a = \tilde{k}_a^0 e^{-\beta \tilde{E}_a^\ddagger(F)} = \frac{S_0 a_s e^{-\beta \tilde{E}_a^\ddagger(F)}}{\sqrt{2\pi m k_B T}} \quad (14)$$

where  $S_0 e^{-\beta \tilde{E}_a^\ddagger(F)}$  is the sticking coefficient for dissociative adsorption at zero coverage [22] (for which we take  $S_0 = 1$ ) and  $\tilde{E}_a^\ddagger(F)$  is the activation energy for the adsorption  $O_2(\text{gas}) \rightarrow 2 O(\text{ad})$ . Moreover, we have [23, 24]

$$\tilde{k}_d = \tilde{k}_d^0 e^{-\beta \tilde{E}_d^\ddagger(F)} = \frac{S_0 a_s k_B T Z_{\text{int}}^{O_2}}{h \lambda_m^2 (q_3^O)^2} e^{-\beta \tilde{E}_d^\ddagger(F)} \quad (15)$$

where  $\tilde{E}_d^\ddagger(F)$  is the activation energy for the desorption  $2 O(\text{ad}) \rightarrow O_2(\text{gas})$  and  $q_3^O$  is the partition function for the center-of-mass vibrations of an adsorbed oxygen atom. We have also introduced  $\lambda_m = h/\sqrt{2\pi m k_B T}$  and  $Z_{\text{int}}^{O_2}$  for, respectively, the thermal wavelength and the partition function of the internal degrees of freedom of the  $O_2$  molecule in the gas phase.

In the absence of carbon monoxide  $P_{CO} = 0$ , the kinetic equation (7) admits the solution

$$\theta_{O, \text{eq}} = \frac{1}{1 + \sqrt{\frac{\tilde{k}_d}{\tilde{k}_a P_{O_2}(F)}}} = \frac{1}{1 + \sqrt{\frac{\tilde{k}_d^0}{\tilde{k}_a^0 P_{O_2}(F=0)} e^{-\frac{\beta}{2} [\tilde{E}_d^\ddagger(F) - \tilde{E}_a^\ddagger(F) + \frac{1}{2} \tilde{\alpha}_{\text{eff}} F^2]}} \quad (16)$$

By imposing detailed balance in Eq. (7), this solution should be the equilibrium one and equal to the value expected from equilibrium statistical mechanics:

$$\theta_{O, \text{eq}} = \frac{1}{1 + e^{\beta(\epsilon_{O, \text{eff}} - \mu_O)}} \quad (17)$$

where  $\epsilon_{O, \text{eff}} - \mu_O$  is the energy difference between the situation with  $O-Au_n$  in an electric field  $F$  and the situation where the chemical potential  $\mu_O$  is fixed, i.e., with  $O-Au_n$  at the electric field  $F$  and an  $O_2$  molecule at the gauge where the partial pressure  $P_{O_2}(F=0)$  is measured. By identification between Eqs. (16) and (17), the effective potential is thus equal to

$$\epsilon_{O, \text{eff}} = -\frac{1}{2} \left[ \tilde{E}_d^\ddagger(F) - \tilde{E}_a^\ddagger(F) + \frac{1}{2} \tilde{\alpha}_{\text{eff}} F^2 \right] \quad (18)$$

On the other hand, we find in terms of the dissociation energies (11)-(13) that

$$\epsilon_{\text{O, eff}} = -V_e(\text{O-Au}_n; F) + \frac{1}{2}D_e(\text{O}_2; F = 0) \quad (19)$$

$$= -V_e(\text{O-Au}_n; F) + \frac{1}{2} \left[ D_e(\text{O}_2; F) - \frac{1}{2}\tilde{\alpha}_{\text{eff}}F^2 \right] \quad (20)$$

where the  $\text{O}_2$  molecule is here supposed to take random orientations with respect to the electric field according to its thermal distribution. Comparing with Eq. (18), we infer that the difference between the activation energies of adsorption and desorption is given by

$$\tilde{E}_d^\ddagger(F) - \tilde{E}_a^\ddagger(F) = 2V_e(\text{O-Au}_n; F) - D_e(\text{O}_2; F) \quad (21)$$

which can be obtained from the DFT data in Fig. 5. We remark that a similar conclusion to that made in Eq. (21) was made previously in the literature when an adsorption barrier is present [22, 23]. Figure 6 depicts this difference obtained from a DFT calculation and its fit to a cubic polynomial:

$$\tilde{E}_d^\ddagger(F) - \tilde{E}_a^\ddagger(F) = -0.7 - 0.25F - 0.005F^2 + 0.0005F^3 \quad (\text{eV}) \quad (22)$$

for an electric field in V/nm.

In a vanishing electric field, the energy barrier for desorption is known from TPD experiments on a single crystal surface [19]

$$\tilde{E}_d^\ddagger(F = 0) = 140 \text{ kJ/mol} = 1.45 \text{ eV} \quad (23)$$

so that the energy barrier for adsorption should be

$$\tilde{E}_a^\ddagger(F = 0) = 2.15 \text{ eV} \quad (24)$$

This value is somewhat smaller than the one obtained using the nudge elastic band method (3.10 eV) [8] on a gold cluster of six atoms. One possible reason for the difference between the two values is from the fact that adsorbates bind more strongly to clusters than to single crystal surfaces resulting in a larger desorption energy and, consequently, a larger activation energy.

To be consistent with our nine atom gold cluster calculations, the energy barrier  $\tilde{E}_a^\ddagger(F)$  for dissociative adsorption should decrease to a minimum value at some negative electric field below the critical value  $F_c \simeq -2.7$  V/nm. In the range  $-10 \text{ V/nm} < F < +10 \text{ V/nm}$ , this requirement is modeled by fitting our DFT calculations to two cubic polynomials

$$\tilde{E}_a^\ddagger(F) = 2.15 + 0.53F + 0.0175F^2 - 0.0023F^3 \quad (\text{eV}) \quad (25)$$

$$\tilde{E}_d^\ddagger(F) = 1.45 + 0.28F + 0.0125F^2 - 0.0018F^3 \quad (\text{eV}) \quad (26)$$

for an electric field in V/nm (see Fig. 6). As required,  $\tilde{E}_a^\ddagger(F) > \tilde{E}_d^\ddagger(F)$  for  $F > F_c$ , while  $\tilde{E}_a^\ddagger(F) < \tilde{E}_d^\ddagger(F)$  for  $F < F_c$  with  $\tilde{E}_a^\ddagger(F)$  reaching a minimum energy for some negative electric field  $F_{\text{min}} < F_c < 0$ . We remark that this is the same qualitative trend that was calculated by Landman *et al.* [8]. Indeed, they obtained an activation barrier of 3.15 eV for  $\text{Au}_6\text{O}_2^+$  which is decreased to 1.27 eV for  $\text{Au}_6\text{O}_2^-$ , which would correspond to having the cluster in a positive and negative electric field respectively.

Let us now determine the prefactors appearing in Eqs. (14) and (15). The constant  $\tilde{k}_d^0$  is adjusted to reproduce TPD data in zero electric field, which is simulated in the present model by the equation

$$\frac{d\theta_{\text{O}}}{dt} = -2\tilde{k}_d\theta_{\text{O}}^2 \quad \text{with} \quad T = T_0 + \gamma t \quad (27)$$

and  $\tilde{k}_d = \tilde{k}_d^0 \exp \left[ -\tilde{E}_d^\ddagger(F = 0)/k_{\text{B}}T \right]$ . The TPD spectra of atomic oxygen on Au(110) presents a peak at 553 K for a heating rate of  $\gamma = 2.015$  K/s [19]. This peak corresponds to the desorption energy (23). It is reproduced in the limit  $\theta_{\text{O}}(t = 0) \rightarrow 0$  by taking the value  $\tilde{k}_d^0 = 9 \times 10^{12} \text{ s}^{-1}$  in Eq. (15). We remark that this peak is relatively insensitive to the geometry of the substrate since a peak at 550 K was observed on Au(111) when a heating rate of 10 K/s was applied [25]. On the other hand, the adsorption rate constant,  $\tilde{k}_a^0$ , in Eq. (14) is estimated to be  $500 \text{ Pa}^{-1} \text{ s}^{-1}$  at 300 K.

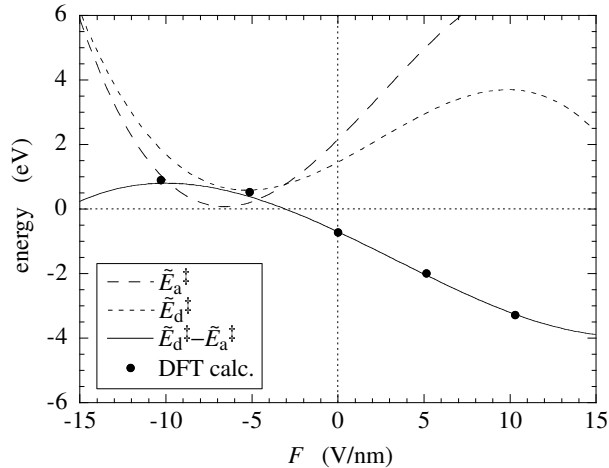


FIG. 6: The energy barriers for dissociative adsorption (25) (long-dashed line) and desorption (26) (dashed line) together with their difference (22) (continuous line) and the corresponding values from DFT calculations (circles).

#### IV. ADSORPTION AND DESORPTION OF CO

CO is a strongly bounded molecule with an electronic dissociation energy of  $D_e = 11.2$  eV in its ground  $X^1\Sigma^+$  singlet electronic state [26, 27], which explains that it does not dissociate upon adsorption on Au since its electronic binding energy is much smaller (in the absence of an electric field, around 0.5-0.6 eV). It has a small electric dipole of 0.11 Debye with oxygen slightly positive in spite of the electronegativity of oxygen.

The electronic binding energy of CO with gold increases in a positive electric field, i.e., an electric field pointing outside the gold cluster and essentially perpendicular to its surface. This binding energy has been calculated elsewhere [11] as a function of the electric field from the energy difference

$$V_e(\text{CO-Au}_n; F) = E(\text{CO}; F) + E(\text{Au}_n; F) - E(\text{CO-Au}_n; F) \quad (28)$$

The desorption energy of CO is thus given by (assuming no activation barrier)

$$E_d^\ddagger(F) = V_e(\text{CO-Au}_n; F) = 0.55 + 0.055 F + 0.0048 F^2 \quad (\text{eV}) \quad (29)$$

with  $F$  in V/nm and  $E_d^\ddagger$  in eV [11]. The rate constant of CO desorption is thus taken as

$$k_d = k_d^0 e^{-\beta E_d^\ddagger(F)} \quad (30)$$

The constant  $k_d^0$  is adjusted to TPD data in zero electric field, which is simulated in the present model by the equation

$$\frac{d\theta_{\text{CO}}}{dt} = -k_d \theta_{\text{CO}} \quad \text{with} \quad T = T_0 + \gamma t \quad (31)$$

with  $k_d$  given by Eqs. (29)-(30). The TPD spectra display a peak at a temperature of 184 K for the heating rate  $\gamma = 1.25$  K/s for a disordered gold surface [19]. This observation leads to the value  $k_d^0 = 2.78 \times 10^{14} \text{ s}^{-1}$  in Eq. (30).

Finally, the adsorption rate constant is taken from Ref. [11]:

$$k_a = 700 \text{ Pa}^{-1} \text{ s}^{-1} \quad (32)$$

at 300 K.

In the absence of oxygen  $\theta_{\text{O}} = 0$ , the solution of the kinetic equation (8) must converge towards the equilibrium stationary solution since detailed balance is imposed

$$\theta_{\text{CO}, \text{eq}} = \frac{1}{1 + \frac{k_d}{k_a P_{\text{CO}}(F)}} = \frac{1}{1 + \frac{k_d e^{-\frac{\beta}{2} \alpha_{\text{eff}} F^2}}{k_a P_{\text{CO}}(F=0)}} = \frac{1}{1 + e^{\beta(\epsilon_{\text{CO}, \text{eff}} - \mu_{\text{CO}})}} \quad (33)$$

The chemical potential  $\mu_{\text{CO}}$  is evaluated where the pressure,  $P_{\text{CO}}(F = 0)$ , has a vanishing electric field. The effective binding potential  $\epsilon_{\text{CO, eff}}$  of CO to the surface is consistently given by

$$\epsilon_{\text{CO, eff}} = -E_{\text{d}}^{\ddagger}(F) - \frac{1}{2} \alpha_{\text{eff}} F^2 \quad (34)$$

with  $\alpha_{\text{eff}} = 0.0014 \text{ eV (V/nm)}^{-2}$ . This is the energy well for a CO molecule bounded at the surface where an electric field,  $F$ , is applied coming from the gauge where the pressure is  $P_{\text{CO}}(F = 0)$ .

## V. CO ADSORPTION WAVE

The CO/O<sub>2</sub>/Au system has been experimentally observed at ultra low pressure in FIM with an *in situ* chemical probe monitoring the ionic species emitted by the surface during the process [10, 11].

The needle of the FIM is made of gold. Under FIM conditions, the needle is positively charged and the electric field at the apex is estimated to be  $F_0 \simeq 12 \text{ V/nm}$ . The needle is first submitted to a pressure of oxygen of  $P_{\text{O}_2} \simeq 10^{-4} \text{ mbar} = 10^{-2} \text{ Pa}$ . Oxygen does not adsorb on positively charged gold so that the gold surface remains essentially empty [10]. Thereafter, CO gas is inlet in the gas phase above the surface with a partial pressure  $P_{\text{CO}} \simeq 2 \times 10^{-7} \text{ mbar} = 2 \times 10^{-5} \text{ Pa}$ . From this initial condition, the propagation of a wave is observed which starts from a point close to the apex where the electric field is the highest and which propagates outward to stop at some distance [11]. The wave stops to propagate at a distance of the order of the radius of curvature where the electric field has dropped to a small value. The *in situ* chemical probe shows that charged gold carbonyls  $\text{AuCO}^+$ ,  $\text{Au}(\text{CO})_2^+$  and  $\text{AuCO}^{2+}$ ,  $\text{Au}(\text{CO})_2^{2+}$  are emitted at the passage of the wave front [9]. This is evidence of the adsorption of CO on the gold surface at the passage of the wave. It has also been concluded that oxygen serves the role of an imaging gas and that the wave front cannot be observed without its presence even if it does not participate in the reaction. Moreover, the adsorption of CO on the edge of a terrace was deduced, because of the local increase in the electric field in these regions.

These observations are explained in terms of the model described in the previous sections as a wave of CO adsorption in a positive electric field without oxygen on the surface [10, 11]. If  $\theta_{\text{O}} \simeq 0$ , Eqs. (7) and (8) of the model reduce to the sole Eq. (8) which has already been shown in Ref. [11] to describe the propagation of the wave. The adsorption of CO is favored by a positive electric field because the binding energy of CO on gold increases above one electron-Volt in the high positive electric field of the FIM.

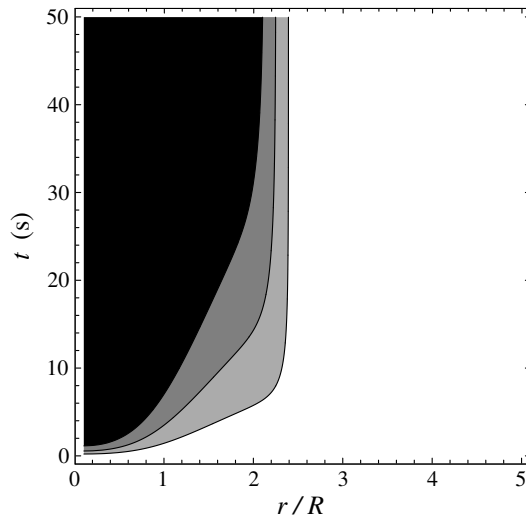


FIG. 7: Space-time plot of CO coverage  $\theta_{\text{CO}}$  as simulated by the theoretical model. The contours are at  $\theta_{\text{CO}} = 0.25, 0.5,$  and  $0.75 \text{ ML}$ . Position  $r$  is in units of the radius of curvature  $R$  and time  $t$  in seconds. The conditions are  $P_{\text{O}_2} \simeq 10^{-4} \text{ mbar} = 10^{-2} \text{ Pa}$ ,  $P_{\text{CO}} \simeq 2 \times 10^{-7} \text{ mbar} = 2 \times 10^{-5} \text{ Pa}$ , and  $F_0 = 12 \text{ V/nm}$ . The initial conditions are  $\theta_{\text{CO}} = 0$  and  $\theta_{\text{O}} \simeq 0$ .

The experimental procedure used to obtain the measured wave propagation on a Au tip can also be simulated using the equations of our model. A preliminary simulation is performed with a bare substrate in a positive electric field (1) with  $F_0 = 12 \text{ V/nm}$  with the pressures  $P_{\text{O}_2} = 10^{-2} \text{ Pa}$  and  $P_{\text{CO}} = 0$ . The surface remains essentially unchanged with  $\theta_{\text{CO}} = 0$  and  $\theta_{\text{O}} \simeq 0$ , which forms the initial conditions for the simulation starting now with the partial pressures

$P_{O_2} = 10^{-2}$  Pa and  $P_{CO} = 2 \times 10^{-5}$  Pa, always in a positive electric field (1) with  $F_0 = 12$  V/nm. The region of the gold surface covered by CO increases and extends in time as depicted in the space-time plot of Fig. 7. The coverage is significant only around the apex of the needle where the electric field is positive and sufficiently large to bind CO on gold, as observed experimentally [11]. The wave front (taken to where  $\theta_{CO} = 1/2$  ML) stops at some distance of the apex where the electric field drops to a negligible value. In the long time limit, the system will reach a stationary regime of thermodynamic equilibrium since the reaction of CO oxidation is completely negligible in a positive electric field. The extension of the region covered with CO can thus be calculated from the condition that  $\theta_{CO,eq} = 1/2$  ML with Eq. (33). The results are depicted in Fig. 8 as a function of CO pressure. The higher the CO pressure, the larger the region covered with CO, as expected.

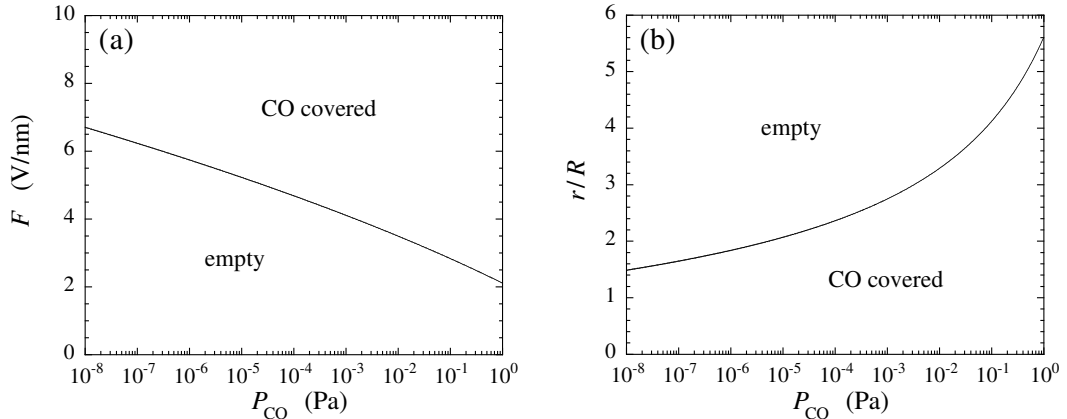


FIG. 8: Values of (a) the electric field  $F$  and (b) the position  $r/R$  of the CO adsorption wave front in the stationary state versus the partial pressure of CO. The field at the apex is  $F_0 = 12$  V/nm,  $T = 300$  K. Since the tip is not covered by oxygen at such positive electric fields, the position of the CO adsorption wave front can be calculated with Eq. (33) which holds for  $\theta_O = 0$ .

The model thus reproduces the experimental observations of the CO/O<sub>2</sub>/Au system in a positive electric field and at ultra low pressures: That a wave of CO adsorption propagates on the FIM tip and that the dissociative adsorption of oxygen is not possible in a positive electric field so that the oxidation of CO does not occur in this case [10, 11].

## VI. CO OXIDATION

Our aim is now to investigate what happens if the electric field turns negative. As alluded in Sec. III, the dissociative adsorption of oxygen could become possible if the electric field is negative and below the critical value  $F_c = -2.7$  V/nm. In this case, we here show that the oxidation of CO does occur at least if the partial pressures of CO and O<sub>2</sub> are sufficiently high.

An example is depicted in Fig. 9 for the apex electric field  $F_0 = -5$  V/nm, where we obtain the tip to be covered by CO molecules and O atoms in sufficient amounts to allow the oxidation of CO. The system is here in a nonequilibrium steady state, which has been reached after relaxation over a long enough time. In this nonequilibrium steady state, the reaction of CO oxidation consumes oxygen and carbon monoxide, and CO<sub>2</sub> is produced at the tip of the needle. The system does not equilibrate since the CO<sub>2</sub> product is rapidly evacuated, which is expressed by its vanishing pressure,  $P_{CO_2} = 0$ . The reactant pressures have been set in a ratio of  $P_{O_2} : P_{CO} = 5 : 1$  (887 Pa and 443 Pa respectively) and the temperature has been set to 300 K, as in the experiments of Ref. [2]. As can be seen in Fig. 9, the atomic oxygen coverage is now important while the CO coverage is moderately reduced by a negative electric field. The latter being due to the small decrease of  $V_e(\text{CO-Au}_9; F)$  with respect to its value at a vanishing electric field [11]. This results in a local yield of CO oxidation,  $k_r \theta_{CO} \theta_O$ , which varies as a function of the radial distance  $r/R$  and which is a maximum at the apex of the tip where the coverage by oxygen is the largest.

Let us now examine how the total yield, as given by Eq. (9), varies as function of the external electric field at the apex of the tip in the nonequilibrium steady state. This is depicted in Fig. 10, where we have used the same temperature and partial pressures as in Fig. 9. We see that the oxidation of CO becomes significant only if the electric field is sufficiently negative. The transition is rather abrupt as a function of the electric field because the process is energetically impossible above the critical electric field.

On the other hand, we can also examine this oxidation dependence on the total pressure,  $P_{tot} = P_{CO} + P_{O_2}$ , when

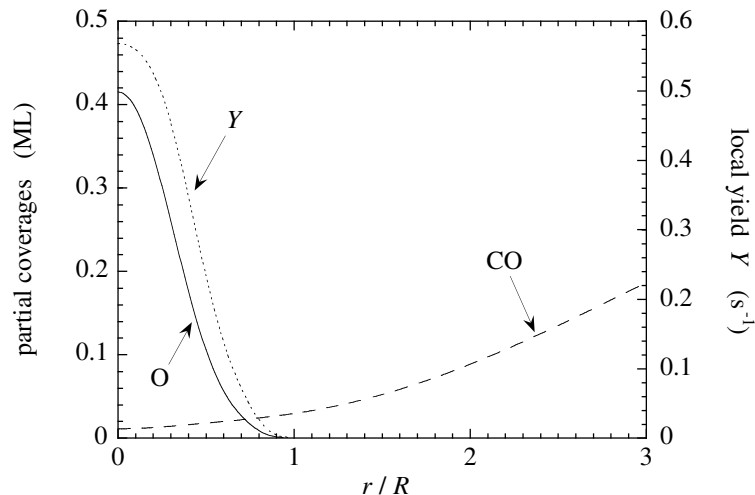


FIG. 9: The partial coverages of CO ( $\theta_{\text{CO}}$ , solid line), atomic oxygen ( $\theta_{\text{O}}$ , dashed line) as a function of the radial distance  $r/R$  on a negatively charged nanotip in a nonequilibrium steady state. The local yield dependence ( $Y = k_r \theta_{\text{CO}} \theta_{\text{O}}$ , dotted line) is also depicted. The partial pressures have been set to  $P_{\text{CO}} = 887$  Pa and  $P_{\text{O}_2} = 4433$  Pa =  $5P_{\text{CO}}$ . The electric field at the apex is equal to  $F_0 = -5$  V/nm and a uniform temperature of 300 K was used.

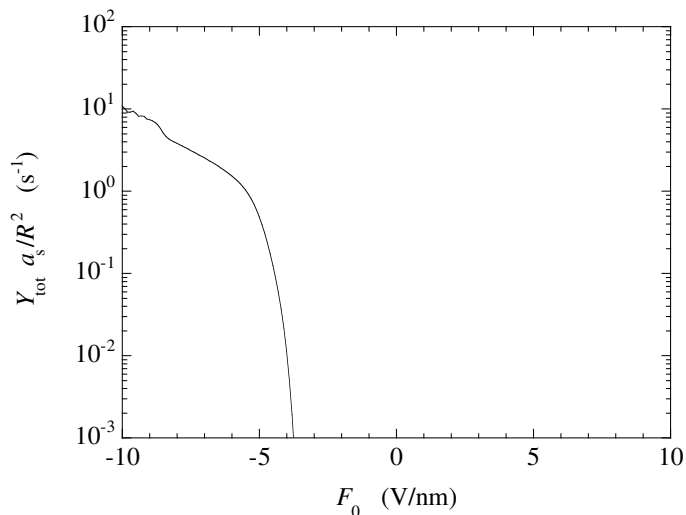


FIG. 10: Total yield of CO oxidation (9) scaled by  $R^2/a_s$  versus the electric field  $F_0$  at apex. The partial pressures and the temperature are as in Fig. 9.

keeping  $P_{\text{O}_2} : P_{\text{CO}}$  in a ratio of 5 : 1, as in the experiments of Ref. [2]. This is shown in Fig. 11 where the electric field at the apex,  $F_0$ , has been set to  $-5$  V/nm. As can be seen in the figure, the total yield varies by ten orders of magnitude when the total pressure varies from  $10^{-2}$  to  $10^5$  Pa in an almost linear fashion when plotted on logarithm scales. We also observe that the total yield becomes significant only if the total pressure is high enough ( $10^4$  Pa). CO oxidation would thus remain very small in experiments with a negative electric field at ultra low pressures as in a FEM.

Finally, one can summarize the above results by doing a contour plot of the total yield as a function of the total pressure and the external electric field ( $P_{\text{tot}}$ ,  $F_0$  respectively) when keeping  $P_{\text{O}_2} : P_{\text{CO}} = 5 : 1$ , as shown in Fig. 12(a). This confirms the remarkable prediction of the present model: That the oxidation of CO is possible at the high pressures  $P_{\text{tot}} = P_{\text{CO}} + P_{\text{O}_2} = 40$  Torr = 5320 Pa of Ref. [2]. Let us now look at the total yield when the ratio of the partial pressures is varied, which, as far as the authors know, has so far not been explored experimentally. This is examined in Fig. 12(b) which depicts the total yield in the plane of the partial pressures ( $P_{\text{O}_2}$ ,  $P_{\text{CO}}$ ). Interestingly, this indicates that our model does not need to have the experimental ratios of the partial pressures to get a significant yield. It would thus be also interesting to know if the same conclusions would apply when examining the CO oxidation

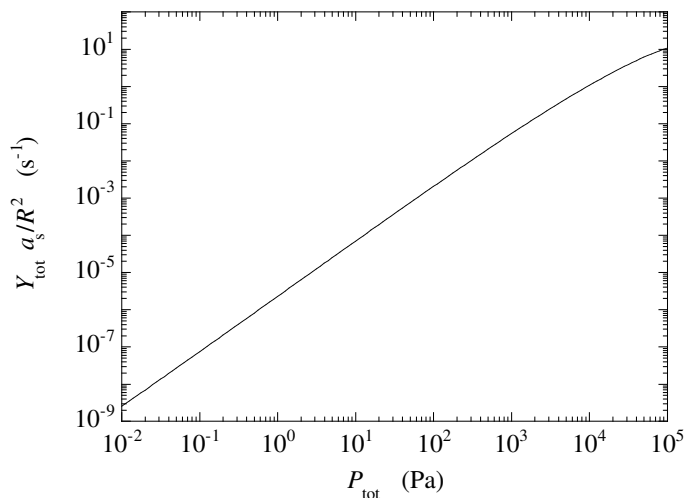


FIG. 11: Total yield of CO oxidation (9) scaled by  $R^2/a_s$  versus the total pressure  $P_{\text{tot}} = P_{\text{CO}} + P_{\text{O}_2}$  while keeping the ratio  $P_{\text{O}_2} = 5P_{\text{CO}}$ . The electric field and temperature are as in Fig. 9.

process on Au clusters supported on a metal oxide.

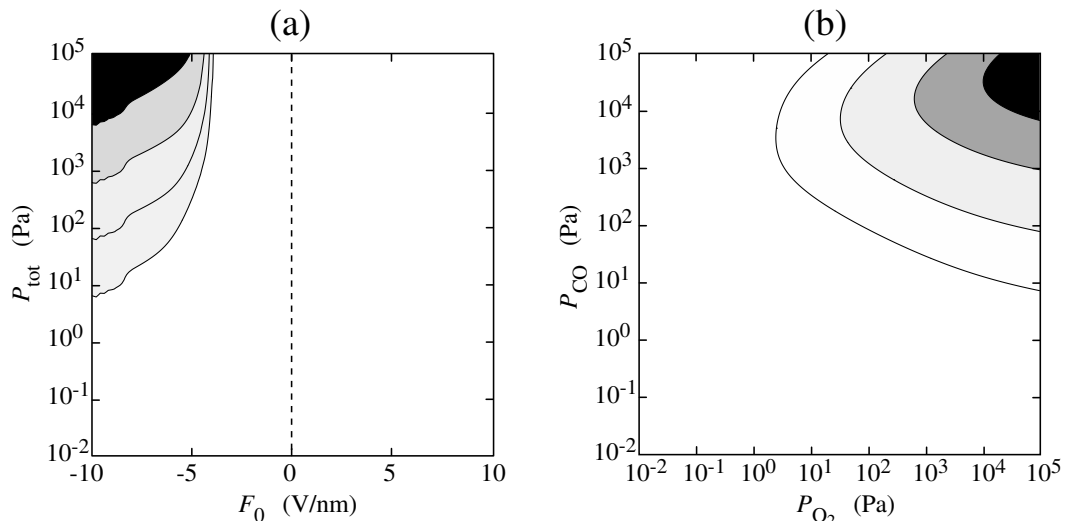


FIG. 12: (a) Contour plot of the total yield of CO oxidation (9) scaled by  $R^2/a_s$  in the plane of the total pressure  $P_{\text{tot}}$  versus the electric field at the apex  $F_0$ , for  $P_{\text{O}_2} = 5P_{\text{CO}}$  with  $T = 300$  K. The contour lines are taken at 0.01, 0.1, 1, and  $10 \text{ s}^{-1}$ . The maximum value is  $121.7 \text{ s}^{-1}$  in the darkest zone. (b) Contour plot of the total yield in the plane of the partial pressures  $P_{\text{O}_2}$  and  $P_{\text{CO}}$  for the electric field  $F_0 = -5 \text{ V/nm}$  and with  $T = 300$  K. The contour lines are taken at 0.01, 0.1, 1, and  $5 \text{ s}^{-1}$ . The maximum value is  $17 \text{ s}^{-1}$  in the darkest zone.

## VII. CONCLUSIONS

In the present paper, we make the prediction that the oxidation of CO is induced on gold by a negative electric field. This prediction is based on DFT calculations of the binding energy of oxygen on gold clusters as a function of the electric field. These DFT calculations show that the dissociative adsorption of oxygen is possible on gold in the presence of a sufficiently negative electric field. For a small cluster  $\text{Au}_9$ , the negative critical value is estimated as  $F_c \simeq -2.7 \text{ V/nm}$ . The consequences of this result have been studied by setting up a kinetic model of CO oxidation based on the Langmuir-Hinshelwood mechanism. The rate constants of the model depend on the electric field, which allows us to investigate the reaction yield for different values of the electric field and gas pressures.

First of all, the model reproduces the experimentally observed wave of CO adsorption followed by carbonyl formation if the electric field is positive and the partial pressures of CO and O<sub>2</sub> are low [11]. Moreover, the model confirms that the dissociative adsorption of oxygen does not happen under these conditions [10].

If the electric field is negative and below the critical value  $F_c \simeq -2.7$  V/nm and, furthermore, if the partial pressures are high enough, the model predicts that the dissociative adsorption of oxygen becomes possible, which switches on the CO oxidation.

The DFT calculations show that the dissociative adsorption of oxygen (and thus CO oxidation) becomes possible if the electric field is negative, which is consistent with other theoretical studies which show that gold clusters on metal oxides such as MgO can be negatively charged [5, 6]. These negative charges should be coming from oxygen vacancies on the surface of the oxide. These vacancies are known to be F centers where electrons are trapped. Gold atoms tend to adsorb and cluster preferentially on these vacancies, leading in this way to negatively charged gold clusters [3, 5, 6]. In this case, they could be surrounded by a negative electric field which would activate the dissociative adsorption of oxygen, leading to CO oxidation.

Further work is required in order to explain the activation of oxygen on gold by the presence of negative electric fields. First, the negative critical electric field is here estimated on a relatively small gold cluster Au<sub>9</sub> by DFT calculations, which should be improved by a more systematic investigation of the way the negative critical electric field depends on the size  $n$  of the cluster Au <sub>$n$</sub> . In this regard, we notice that Fig. 5 suggests that the negative critical electric field tends to decrease in absolute value as the cluster size increases ( $F_c \simeq 13.4$  V/nm for  $n = 1$ ) so that a less negative value than  $F_c \simeq -2.7$  V/nm is likely. There also remains the important question of estimating the charging of a gold nanocluster supported on a metal oxide. The distribution of the electric charge around the nanocluster depends on its shape and should determine the electric field on its surface [see Fig. 1(c)]. In this regard, the yield of CO oxidation on gold nanoclusters could thus be obtained in terms of the kinetic model developed in the present paper.

Finally, an extension of the present model is also foreseeable by allowing the molecular adsorption process of O<sub>2</sub> onto the gold cluster, which would then react to form a CO<sub>2</sub> molecule and a O atom. Indeed, Landman *et al.* [5, 6, 8] have shown that the adsorption energy of O<sub>2</sub> becomes significant when it adsorbs on a gold cluster that is negatively charged. They also calculated the activation barrier to dissociate an adsorbed O<sub>2</sub> molecule, which they have determined to become smaller when the cluster becomes negatively charged [8]. To take this oxidation process into account along with the one used in the paper one would have to use the theoretical development in Ref. [23]. Taking into account this other reaction pathway would no doubt increase the yield of CO<sub>2</sub>, which was calculated in Sec. VI. Thus, the yields calculated in the present paper can be regarded more as lower bounds. Moreover, when the gold cluster is supported on a metal oxide, this alternative oxidation process has been determined to be much more favorable than the one considered in the present paper [4], which indicates that the electric fields around the supported Au cluster are *perhaps* not as strong as the minimum value needed in the present model. We hope to report on these issues in a future publication.

**Acknowledgments.** The authors would like to thank Norbert Kruse, Thierry Visart de Bocarmé, and Hans Jürgen Kreuzer for useful comments. This research is financially supported by the “Communauté française de Belgique” (contract “Actions de Recherche Concertées” No. 04/09-312).

- 
- [1] M. Haruta, *Catal. Today* **36**, 153 (1997).
  - [2] M. Valden, X. Lai, and D. W. Goodman, *Science* **281**, 1647 (1998). Appearance of Nonmetallic Properties
  - [3] R. Meyer, C. Lemire, Sh. K. Shaikhutdinov, and H.-J. Freund, *Gold Bulletin* **37**, 72 (2004).
  - [4] L. M. Molina and B. Hammer, *Appl. Catal. A* **291**, 21 (2005). catalytic activity of Au
  - [5] A. Sanchez, S. Abbet, U. Heiz, W.-D. Schneider, H. Häkkinen, R. N. Barnett, and U. Landman, *J. Phys. Chem. A* **103**, 9573 (1999).
  - [6] B. Yoon, H. Häkkinen, U. Landman, A. S. Wörz, J.-M. Antonietti, S. Abbet, K. Judai, and U. Heiz, *Science* **307**, 403 (2005). Clusters on MgO
  - [7] Z.-P. Liu, X.-Q. Gong, J. Kohanoff, C. Sanchez, and P. Hu, *Phys. Rev. Lett.* **91**, 266102 (2003). Principles Study of CO oxidation on TiO<sub>2</sub> Supported Au
  - [8] B. Yoon, H. Häkkinen, and U. Landman, *J. Phys. Chem. A* **107**, 4066 (2003).
  - [9] T.-D. Chau, T. Visart de Bocarmé, N. Kruse, R. L. C. Wang, and H. J. Kreuzer, *J. Chem. Phys.* **119**, 12605 (2003). gold nanostructures
  - [10] T. Visart de Bocarmé, T.-D. Chau, F. Tielens, J. Andrés, P. Gaspard, R. L. C. Wang, H. J. Kreuzer, and N. Kruse, *J. Chem. Phys.* **125** 054703 (2006).
  - [11] T. Visart de Bocarmé, N. Kruse, P. Gaspard, and H. J. Kreuzer, *J. Chem. Phys.* **125** 054704 (2006).
  - [12] R. H. Good and E. W. Müller in *Encyclopedia of Physics*, Vol. XXI, edited by S. Flügge, (Springer-Verlag, Berlin, 1956), pp. 176-231.

- [13] R. Gomer, *Field Emission and Field Ionization* (Harvard University Press, Cambridge, MA, 1961).
- [14] M. K. Miller, A. Cerezo, M. G. Hetherington and G. D. W. Smith, *Atom Probe Field Ion Microscopy*, Monographs on the Physics and Chemistry of Materials (Clarendon Press, Oxford, 1996).
- [15] E. A. Guggenheim, in *Encyclopedia of Physics*, Vol. III/2, edited by S. Flügge (Springer-Verlag, Berlin, 1959), pp. 1-118.
- [16] J.-S. McEwen and P. Gaspard, unpublished.
- [17] N. D. Bridge and A. D. Buckingham, Proc. R. Soc. Lon. Ser. A **295**, 334 (1966).
- [18] S. H. Payne, A. Wierzbicki, and H. J. Kreuzer, Surf. Sci. **291**, 242 (1993).
- [19] J. M. Gottfried, *CO oxidation over gold: Adsorption and reaction of oxygen, carbon monoxide, and carbon dioxide on an Au(110)-(1×2) surface* (Ph. D. thesis, Freien Universität Berlin, 2003).
- [20] T.-D. Chau, *Réactions chimiques sur surfaces de platine et d'or à l'échelle atomique: Approche théorique et expérimentale* (Ph. D. thesis, Université Libre de Bruxelles, 2004).
- [21] F. Tielens, J. Andrés, T.-D. Chau, T. Visart de Bocarmé, N. Kruse and P. Geerlings, Chem. Phys. Lett. **421**, 433 (2006).
- [22] W. Brenig, H. J. Kreuzer, and S. H. Payne, Phys. Rev. B **67**, 205419 (2003).
- [23] H. J. Kreuzer, S. H. Payne, D. Drozdowski, and D. Menzel, J. Chem. Phys. **110**, 6982 (1999).
- [24] H. J. Kreuzer and S. H. Payne, in *Computational Methods in Surface and Colloid* edited by M. Borowko, (Marcel Dekker Inc., New York, 2000).
- [25] X. Deng, B. K. Min, A. Guloy, and C. M. Friend, J. Am. Chem. Soc. **127**, 9267 (2005). Implications for oxygen catalysis
- [26] P. G. Hajigeorgiou and R. J. Le Roy, J. Chem. Phys. **112**, 3949 (2000).
- [27] Y. Huang and R. J. Le Roy, J. Chem. Phys. **119**, 7398 (2003).